Significance of Local Density of States in the Scanning Tunneling Microscopy Imaging of Alkanethiol Self-Assembled Monolayers

Alexandru Riposan and Gang-yu Liu*

Department of Chemistry, University of California, Davis, California 95616

Received: June 16, 2006; In Final Form: September 19, 2006

A systematic scanning tunneling microscopy (STM) study of alkanethiol self-assembled monolayers (SAMs) is presented as a function of the bias voltage, tunneling current, and tip-termini separation. Stable and etch-pit free SAMs of close-packed undecanethiol/Au(111) were obtained after annealing in ultrahigh vacuum. STM revealed two distinct c(4×2) structures with four nonequivalent molecules per unit cell. For both structures, reversible contrast variations occur upon systematically tuning the bias voltage, the current, and the tip−termini distance. These contrast transitions originate from probing the corresponding local density of states (LDOS) of each molecule and not from the reorientation of the alkanethiol chains. The STM contrast is particularly sensitive to the tip−termini separation in the range of 0.5−2.5 Å, reflecting the distance-dependence of LDOS. At a fixed tip elevation, the STM contrast is less sensitive to changes in bias within 0.1−1.2 V. For the first time, we demonstrate that LDOS may override the physical height variations in the STM topographic contrast for alkanethiol SAM systems.

Introduction

Self-assembled monolayers (SAMs)[1] of organic molecules on metal surfaces have attracted much attention due to their potential applications in advanced technology such as molecular electronics,[2−5] nano- and micromechanical systems (NEMS and MEMS),[6−8] chemical and bio-sensing,[9−11] and biotechnology.[12−16] Among the most extensively studied SAM systems are monolayers of alkanethiols on Au(111) surfaces, whose structure has been examined by a variety of experimental techniques, including X-ray,[17−20] electron[21] and helium diffraction,[22,23] FTIR,[24,25] atomic force microscopy (AFM),[26−29] and scanning tunneling microscopy (STM).[29−51] In particular, STM revealed important insights into the physical structure and electronic properties of SAMs with unprecedented resolution.[29−51] At monolayer coverage, alkanethiols form close-packed domains with a commensurate $(\sqrt{3}\times\sqrt{3})$R30° structure with respect to the Au(111) surface. Various c$(4\sqrt{3}\times2\sqrt{3})$R30° superstructures were also observed, referred to as c(4×2).[37,38,49,52] Six contrasts have been reported in prior STM studies, which are summarized schematically in Figure 1, following the notation established in the literature.[37,38,49,52] In all models, the close-packed molecular rows follow the $\langle 1\bar{2}1\rangle$ directions of the Au(111) surface, with a spacing of 0.50 nm between molecules. The $(\sqrt{3}\times\sqrt{3})$R30° structure (Figure 1a) is composed of molecules with equivalent adsorption and configuration, whereas the unit cell of c(4×2) (Figure 1b−f) is composed of nonequivalent molecules displaying up to four levels of brightness in STM topographs. The coexistence of several contrasts (i.e., the $(\sqrt{3}\times\sqrt{3})$R30° and up to three types of c(4×2)) was observed simultaneously in the same scan,[36,37,48,51] suggesting that physically different structures with similar energies are present in alkanethiol SAMs. However, the coexistence of all six STM contrasts (Figure 1) has never been reported. Notably, annealed SAMs exhibit mostly c(4 × 2) contrasts, indicating that the c(4×2) structures are thermodynamically more stable than the $(\sqrt{3}\times\sqrt{3})$R30° lattice.

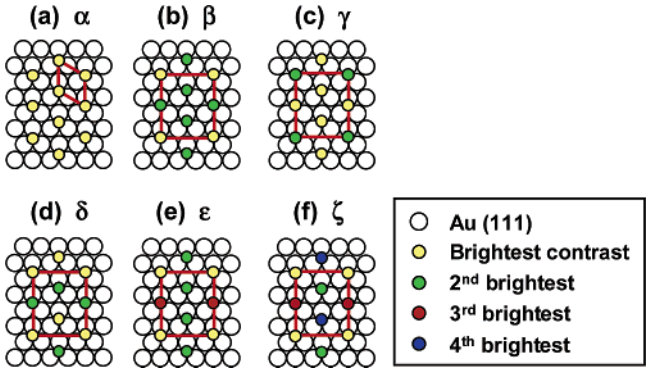

Figure 1. Summary of the STM contrasts reported previously for alkanethiol SAMs. Contrast α represents the $(\sqrt{3}x\sqrt{3})$R30° structure and contrasts $\beta-\zeta$ have the c$(4\sqrt{3}\times2\sqrt{3})$R30° periodicity. For clarity of the illustration, the STM spots corresponding to alkanethiol molecules are represented as located on equivalent triple-hollow adsorption sites (i.e., assuming zero tilt and rotation angles).

Despite the numerous studies of this system, the origin of these contrasts has not been established with certitude. The fundamental question is: does the STM contrast reflect the physical structure of the SAM? The orientation of alkanethiol molecules in close-packed SAMs is shown schematically in Figure 2, as inferred from both experimental[20,24,25] and theoretical[53−55] studies. The molecules adopt an all-trans configuration, with a tilt angle of $\theta = 30°$ from the surface normal toward the next-nearest neighbor direction (NNN or $\langle 110\rangle$).[20] In addition, the chains have a rotation angle $\chi = 5-20°$ of the molecular axis about the surface normal and away from the NNN direction,[20] and a twist angle φ defined as the rotation of the plane containing the zigzag carbon chain around the molecular axis. In Figure 2, $\varphi = 0°$ corresponds to the zigzag plane coinciding with the plane defined by the molecular axis and the surface normal. In the model shown in Figure 2, the sulfur headgroup is assumed to occupy the triple hollow site of Au(111) following the literature convention,[1,32,46,54] although other binding sites remain possible.[1,51,56−64] Theoretical studies[53−55] suggest tens of stable structures, which are described by different

* To whom correspondence should be addressed. E-mail: liu@chem.ucdavis.edu. Phone: 530-754-9678. Fax: 530-754-8557.

10.1021/jp063774w CCC: $33.50
Published on Web 11/09/2006

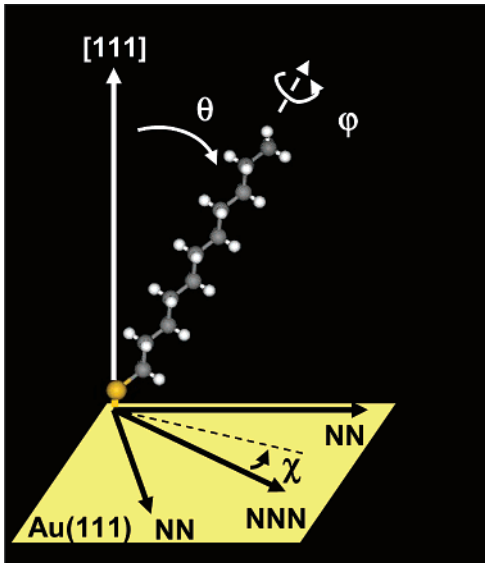

Figure 2. Schematic diagram illustrating the orientation of individual alkanethiol molecules in close-packed structures, where the tilt (θ), rotation (χ) and twist (φ) angles are defined. The large atom at the bottom of the chain represents the sulfur atom. The [111] direction is the surface normal, while NN and NNN represent the nearest neighbor and next-nearest neighbor directions of thiols, respectively. The dotted line is the projection of the alkane chain on the Au surface.

(θ, χ, φ) combinations. For a given c(4×2) structure, the values of θ and χ are fixed, while variations in φ among molecules within the same unit cell result in different physical heights. Then, the question becomes: do the observed STM contrasts (Figure 1) reflect only variations in (θ, χ, φ)?

It has been proposed that the STM contrast of alkanethiols (Figure 1) indicates either the position of the S atoms[40] or that of the top methyl groups.[38,48] In the later case, the c(4×2) brightness modulation would be caused by height differences among molecules with different φ. Indeed, recent noncontact AFM[27] experiments revealed height variations within the unit cells of both δ and ϵ c(4×2) structures. However, recent density functional theory (DFT) studies suggest that, although the physical structure may impact the STM contrast of alkanethiol SAMs, one cannot rule out the influence of local density of states (LDOS).[46,65] Taking into account the LDOS effects, these simulations predicted a dependence of the c(4×2) contrast on bias voltage, adsorption site, S hybridization, chain length, and tip-SAM separation.[46,65] Constant-height STM by Zeng et al.[46] showed variations in the shape and brightness of the molecules comprising a c(4×2) contrast upon changing the bias voltage but not transitions among different types of c(4×2) (e.g., in Figure 1). It was concluded that the STM contrast is dominated by the physical structure of the SAM, although affected in detail by LDOS. In an earlier study, Bucher et al.[39] observed variations in the STM patterns between c(4×2) and ($\sqrt{3}\times\sqrt{3}$)R30° upon changing the tunneling conditions. Pflaum et al. reported a reversible $\gamma \leftrightarrow \delta$ transition for decanethiol SAMs upon changing the bias voltage, which was believed to be due to electronic effects.[45] Many other studies attributed reversible or irreversible changes in the STM contrast to changes in the physical structure of the SAM (i.e., changes in (θ, χ, φ) caused by strong tip-SAM interactions during imaging in air or liquid).[29,50,56]

In this article, we report a systematic investigation of the STM contrast of alkanethiol SAMs under ultrahigh-vacuum (UHV). Using high-resolution imaging, systematic in situ variations in the bias voltage (V), tunneling current (I), and tip-SAM distance, and ($I-V$) spectroscopy, we are able to demonstrate unambiguously the importance of LDOS in the STM imaging of alkanethiols. Our UHV−STM investigation has revealed at least three physically different structures of SAMs, a ($\sqrt{3}\times\sqrt{3}$)R30° and two c(4×2) superlattices. For the two c(4×2) superlattices, we have observed systematic, reproducible, and reversible transitions in the STM contrast upon changing the imaging conditions. These contrast transitions originate from variations in LDOS and not from the reorientation of the alkanethiol chains. For the first time, we demonstrate that the LDOS contribution can override the differences in the physical height of molecules in the STM contrast of alkanethiols, contrary to previous conclusions.[46] This investigation provides new insights into the understanding of the structure and electronic properties of SAMs, as well as into the electron transfer and transport processes of SAM-based molecular electronics.

Experimental Section

All STM images reported in this article were acquired on annealed undecanethiol SAMs on Au(111) surfaces, imaged by ultrahigh vacuum scanning tunneling microscopy (UHV−STM). The Au(111) substrates were prepared by thermal evaporation of Au (Alfa Aesar, 99.999%) onto freshly cleaved mica (0001) surfaces. Typically, 200 nm gold films were deposited at a rate of ~3 Å/s and a substrate temperature of 350 °C, in a high-vacuum evaporator (Denton Vacuum, Inc.) with a base pressure $<1\times10^{-6}$ Torr. Following the metal deposition, the films were annealed in situ at 375 °C for 20 min. Upon cooling to room temperature under vacuum, the films were removed from the deposition chamber and subjected to hydrogen flaming. This procedure produced Au(111) terraces typically 100 nm wide. Undecanethiols of 99% purity were purchased from Aldrich and used without further purification. Freshly prepared Au(111) substrates were immersed into 0.5 mM undecanethiol/ethanol solutions for at least 24 h. Upon the formation of the SAM, the samples were removed from the solution; washed sequentially with ethanol, hexanes, and ethanol; and briefly left to dry in air before being loaded into the UHV−STM system (RHK Technology, Inc.). The SAMs were annealed in UHV at base pressures of 10^{-10} Torr, using a tungsten filament heater mounted underneath the sample stage. Typically, the annealing was done at 345 K for 4−6 h, followed by overnight cooling to room temperature under UHV.

The SAMs were imaged at room temperature (~296 K) at a base pressure below 5×10^{-10} Torr. All STM images shown were acquired at positive bias (sample positive) in high impedance, constant-current mode, using tungsten tips prepared by electrochemical etching in 3 M KOH or NaOH aqueous solutions. Domains of different phases have been scanned repeatedly at bias voltages (V) between +0.1 and +1.2 V and tunneling currents (I) between 2 and 70 pA. The resistance recorded during STM imaging ranged between 13 and 300 GΩ. The imaging conditions surveyed cover the typical range used for the STM imaging of alkanethiol SAMs with this or similar chain lengths.[29−32,34−39,52]

Scanning tunneling spectroscopy (STS) was utilized in the attempt to reveal the LDOS of the SAM.[45,66] The STM tip was carefully placed above designated lattice sites (i.e., individual molecules within the c(4×2) unit cell) at chosen (I,V) setpoints. Then, the feedback was turned off and series of sequential I−V curves were recorded rapidly to eliminate possible variations caused by thermal drift. The absence of drift during the spectroscopic measurements was also verified by comparing high-resolution STM images recorded right before and im-

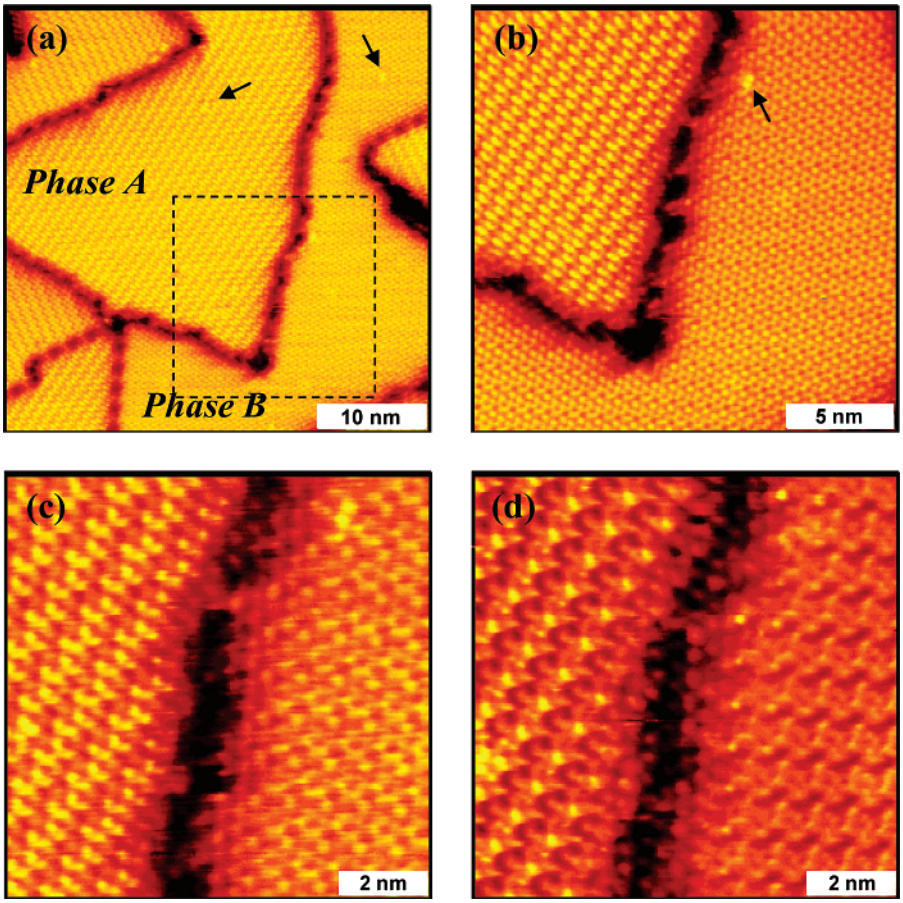

Figure 3. STM topographic images of an undecanethiol SAM, after annealing at 345 K for 4.5 h under UHV. The images were recorded at (a) 0.8 V, 14 pA; (b) 0.8 V, 14 pA; (c) 0.3 V, 5 pA; (d) 0.3 V, 14 pA. Image b was taken inside the square area indicated in panel a, and panels c and d are zoomed-in images of panel b. Point defects in the SAM are indicated by arrows in panels a and b. Two distinct phases, A and B, coexist on the surface, observed simultaneously under the same imaging conditions.

mediately after the STS acquisition. The lateral shift was kept minimal, and the measurements were retaken if the drift was greater than 1 Å. For each type of molecule, the I−V curves recorded at the same setpoint were averaged and lightly smoothened, and converted into dI/dV−V plots.

Results and Discussion

A. Two c(4 × 2) Structures Coexist for Annealed Undecanethiol SAMs. Figure 3a shows a typical STM topograph of an undecanethiol SAM upon UHV annealing at 345 K for 4.5 h. Panels b−d in Figure 3 are zoom-in images within the area marked in Figure 3a. The SAM consists of etch-pit free c(4 × 2) domains up to several hundreds of nanometers in size, with only occasional missing molecules or other point defects. This morphology is different from that of as-deposited undecanethiol SAMs (not shown), which exhibited both small $(\sqrt{3}\times\sqrt{3})$R30° and c(4×2) domains decorated by etch pits, in accordance with previous reports.[30,33,37,38] The absence of the $(\sqrt{3}\times\sqrt{3})$R30° on the annealed surfaces supports the conclusion inferred previously that the c(4×2) structures of alkanethiols are thermodynamically more stable than the basic $(\sqrt{3}\times\sqrt{3})$R30°.[1,27,37,38]

As shown in Figure 3, two distinctively different c(4×2) contrasts are observed simultaneously in adjacent domains under the same imaging conditions. In addition, the STM contrast of each domain varies differently upon changing the imaging V and I. For example, the left-side domain in Figure 3b−d shows a β-contrast in Figure 3d and a ζ contrast in Figure 3b,c. The right-side domain displays mostly a δ contrast with a low brightness in all images. Collectively, these observations indicate that these domains correspond to two different c(4×2) phases (i.e., different physical structures). We emphasize here the terms phase vs contrast: each c(4×2) phase is a structure characterized by a set combination of (θ, χ, φ), whereas a c(4×2) contrast is the STM topographic image displayed by a phase at given imaging conditions (I and V). The two phases observed on these annealed undecanethiol SAMs will be referred to in the following as phase A and phase B, as indicated in Figure 3. The coexistence of at least two different c(4×2) phases has also been inferred from previous STM[36,37,48,51] and AFM[27] studies.

B. Proposed Models for the Two c(4 × 2) Phases. The observation of several c(4×2) contrasts for the same phase, as well as the incertitude surrounding the physical height contribution to the STM contrast, makes the construction of structural models more difficult than in previous approaches, which derived physical structures directly from STM topographs. Nonetheless, attempts were made to construct two models, shown in Figure 4, based on molecular dynamics (MD) simulations by Li et al.[54] and taking into account the combined experimental evidence of this study. The two original structures[54] have nearly the same energy, as expected for coexisting phases. In addition to prior diffraction and spectroscopy studies,[20,24,25] several new observations were taken into consideration in constructing the models. First, under most imaging conditions (sections C and D), phases A and B show mostly ϵ and δ c(4 ×2) contrasts, respectively; thus, the models were built to reflect primarily these symmetries. Second, both phases A and B have four nonequivalent molecules per unit cell, as observed in the high-resolution STM images. Third, the numerous contrast

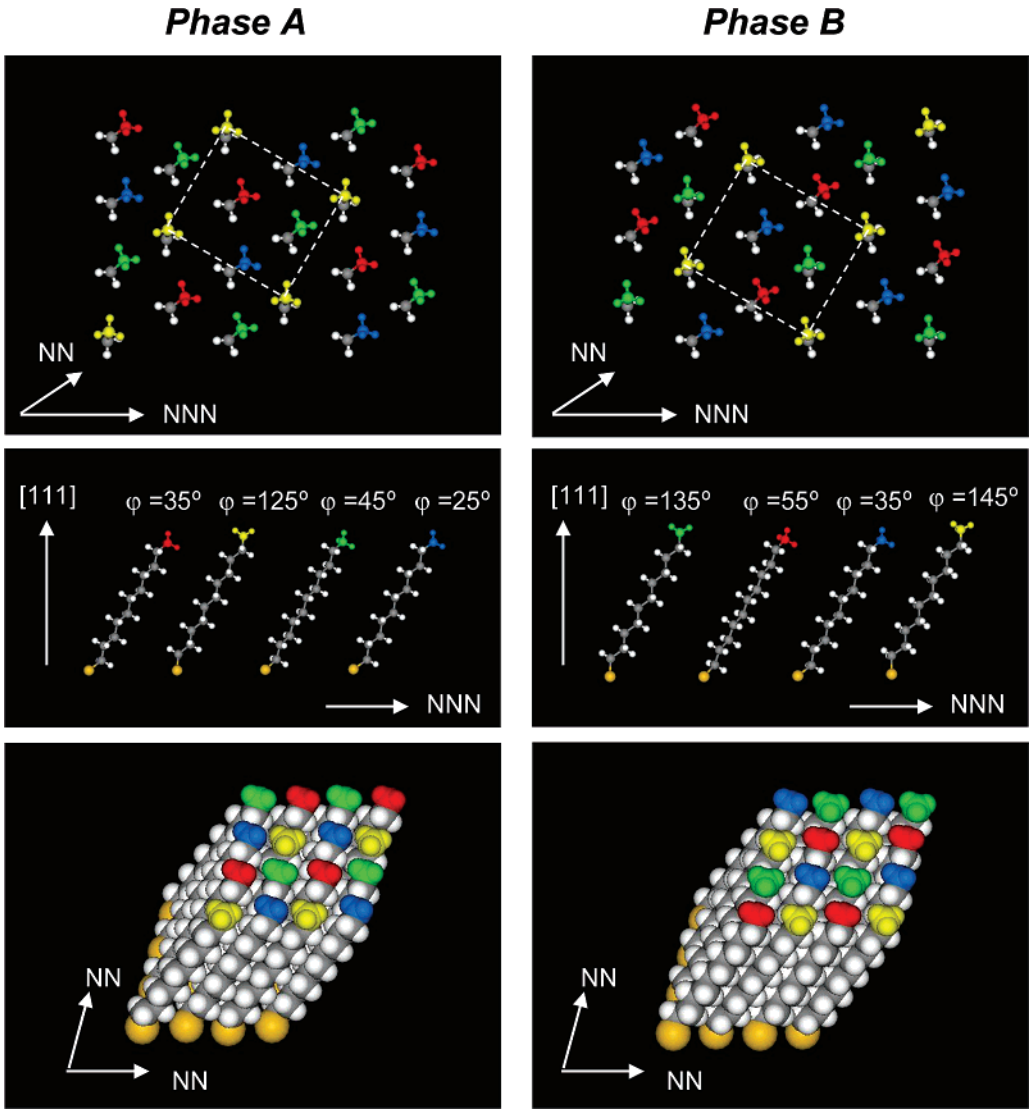

Figure 4. Proposed models for phases A and B, displayed in top, side and 3D views. For simplicity, the Au(111) surface is not shown. The top methyl groups are represented in different colors for nonequivalent molecules. The molecular nearest neighbor (NN) and next-nearest neighbor (NNN) directions are indicated. In the top view, only the terminal methyl and methylene groups are shown. The side view is the plane made by the surface normal [111] and the NNN. $\theta = 30°$ and $\chi = 15°$ for all molecules, while the φ angles are indicated in the diagrams. The unit cell is drawn with the corners on the tallest molecules. Graphic is generated using DS ViewerPro 5.0 (Accelrys, Inc.).

variations observed suggest that the molecules are significantly different in orientation and/or in LDOS. Variations in φ account for the differences in physical height.[53−55] Variations in LDOS within the unit cell may originate from the different hybridization of the S headgroups chemisorbed on the Au(111) surface, according to DFT calculations.[46,65] It is possible that additional variations in φ may alter the LDOS, if they are sufficiently large to alter the chemisorption status of the sulfur.[54,65] Another factor could be the sulfur headgroups occupying nonequivalent sites on Au(111)[46,65] (e.g., triple-hollow, bridge, or atop sites). For simplicity and following the literature's convention,[1,32,39,49,54,55] we use only triple-hollow sites for the construction of the structural models in Figure 4. Simulations are necessary to further refine these models and to verify to what extent the LDOS variations arise from a combination of S hybridization, chain orientation, and nonequivalent adsorption sites.

The resulting model for phase A (Figure 4, left column) consists of four nonequivalent molecules per unit cell, three with sp^3 and one with sp headgroups ("4 chains per unit cell, 3−1 mode").[54] All molecules are tilted $\theta = 30°$ from the surface normal, with a rotation angle $\chi = 15°$ added here based on diffraction experiments.[20] Assuming the same φ values[54] for the three sp^3 molecules, as proposed in the original model, there should only be two kinds of molecules per unit cell resulting in a β-c(4×2) contrast. To account for the four nonequivalent molecules observed in STM (section C), we changed the φ by $\pm 10°$ from the original average values, which is allowed by the stable configuration,[54] resulting in a structure which is more similar to the ϵ-c(4×2). The resulting differences in φ accentuate the differences in height[54] and LDOS[65] among nonequivalent molecules. The model for phase B (Figure 4, right column) is based on a structure proposed for the δ contrast ("4 chains per unit cell, 2−2 mode"),[54] for which the unit cell is composed of two molecules with sp^3 and two with sp chemisorption modes. For this structure, $\theta = 30°$, $\chi = 15°$, and the original values of φ have been modified by $\pm 10°$ to accentuate the differences among nonequivalent molecules. Because of the presence of two twist angles, corresponding to the sp^3 and sp modes, the methyl termini in the c(4×2) structures exhibit both tilted and upright conformations. This differs from the $(\sqrt{3}\text{x}\sqrt{3})\text{R}30°$ structure where all methyl termini share the same orientation

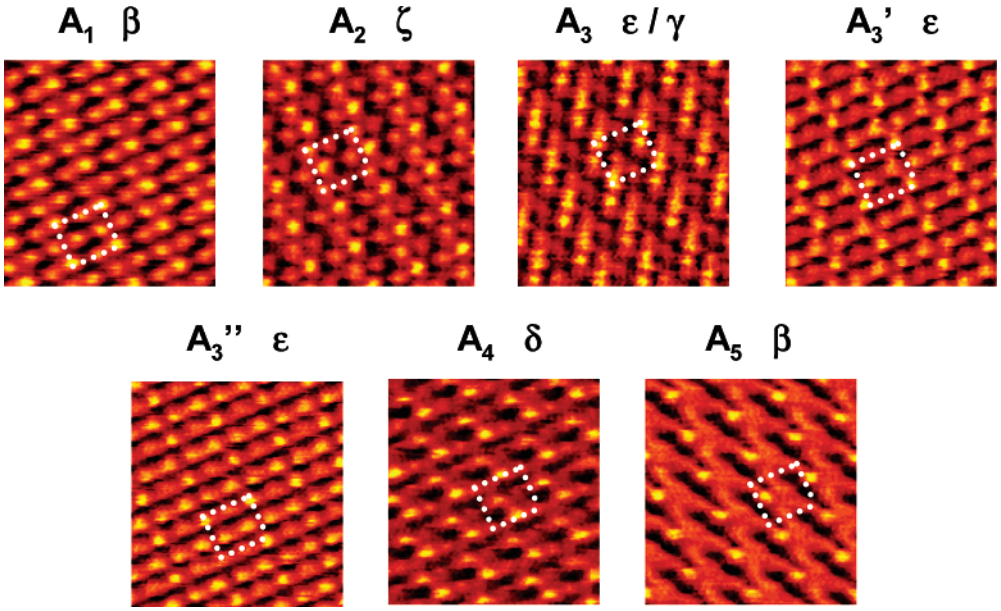

Figure 5. Characteristic STM contrasts observed for *Phase A*, image size 40 Å × 40 Å. The c(4 × 2) unit cell is drawn with the corners on the same of the four nonequivalent molecules for all contrasts shown, as discussed in the text. Three nonequivalent molecules become the brightest in the unit cell, depending on the imaging conditions. A_1 (0.8 V, 6 pA), A_2 (0.8 V, 17 pA), A_3 (0.8 V, 26 pA), A_3' (1.0 V, 49 pA), A_3'' (1.0 V, 63 pA), A_4 (0.8 V, 61 pA), A_5 (0.3 V, 22 pA).

at a given chain length,[54,55] which causes the differences between the even- and odd-carbon SAMs.[1]

C. STM Contrast Variations in Phase A.

C.1. STM Contrast Diagram. Systematic and reversible changes in the c(4×2) STM contrast of phase A have been observed upon changing the bias voltage and/or the tunneling current. Figure 5 shows five characteristic STM topographs observed under defined (*I* and *V*) conditions, displayed in the order of increasing current (decreasing impedance). All images were recorded in the same experiment, within the same domain, and using the same STM tip, but the same contrasts were observed in other experiments as well. All contrasts displayed by this phase are among those reported in the literature (Figure 1). In this figure, the unit cells are drawn with the corners on equivalent molecules for all contrasts; in other words, the corner molecule in A_1 has the same (θ, χ, φ) as in A_2-A_5. The method used to track equivalent molecules among different contrast types will be explained in section C.3. Contrast A_1, observed at the highest impedances used, is qualitatively similar to the β-c(4×2) structure shown in Figure 1b; that is, it consists of one bright and three darker molecules per unit cell. Contrast A_2 is similar to the ζ-c(4×2) scheme shown in Figure 1f. Contrasts A_3, A_3', and A_3'' correspond to the ϵ-c(4×2) shown Figure 1e, with slight variations in the relative apparent heights among molecules within the unit cell. Contrast A_4 is a δ-c(4×2), whereas contrast A_5 is qualitatively a β-c(4×2) observed at the lowest impedances used. In A_1 and A_2, the molecules comprising the long side of the unit cell are spaced at approximately 4.5 and 5.5 Å, deviating from the uniform 5.0 Å spacing observed in the c(4×2) models (Figure 1). A similar observation was made previously for buthanethiols[56] and was attributed to nonequivalent adsorption sites, assuming that the STM detects the S atoms. However, DFT calculations indicated that this deviation can be caused by the STM detection of LDOS maximum located above the terminal methyl groups.[46,65] For example, the irregular spacing in A_1 and A_2 is very similar to that between the methyl groups in the model shown in Figure 4 for phase A, which arises entirely from the twist and rotation of the chains, as the S atoms are regularly spaced. The spacing in this direction appears more regular for the other contrasts, which most likely reflects a shift in the LDOS probed by STM related to the orientation of the terminal C−C bonds.[46,65]

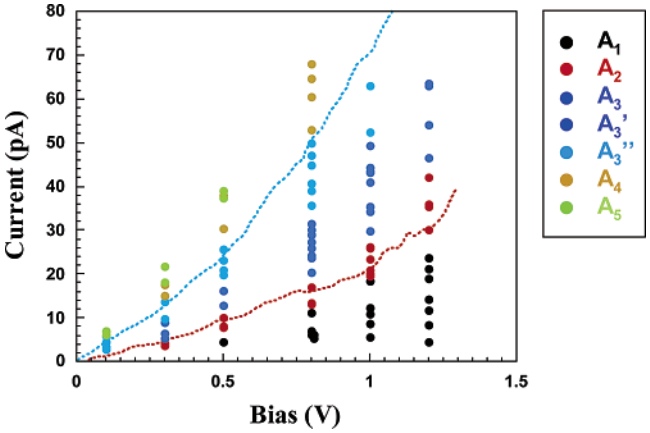

Figure 6. Contrast diagram for phase A as a function of bias and current. The same family of contrasts is represented in the same color. The contrasts of A_3, A_3', and A_3'' are very similar, thus are plotted in similar colors. The red and blue dotted curves are portions of current−voltage (*I*−*V*) spectra taken at the setpoints (0.8 V, 16 pA) and (0.3 V, 10 pA), respectively.

The dependence of the STM contrast on the bias voltage (*V*) and tunneling current (*I*) is summarized in the contrast diagram shown in Figure 6. Every data point in this diagram represents an STM image recorded at the corresponding *V* and *I*. Various c(4×2) contrasts are represented using assigned colors. The dotted curves are portions of current−voltage (*I*−*V*) spectra recorded at the setpoints (0.3 V, 10 pA) and (0.8 V, 16 pA) (see details in section C. 2). Figure 6 clearly indicates that the contrast types are not randomly distributed, but they are organized in separate, well-defined (*I* and *V*) domains, analogous to a phase diagram. Interestingly, at a given bias, there is a systematic progression of contrast types with increasing current and the same sequence is followed at each bias. Moreover, the same progression is followed when decreas-ing the bias voltage

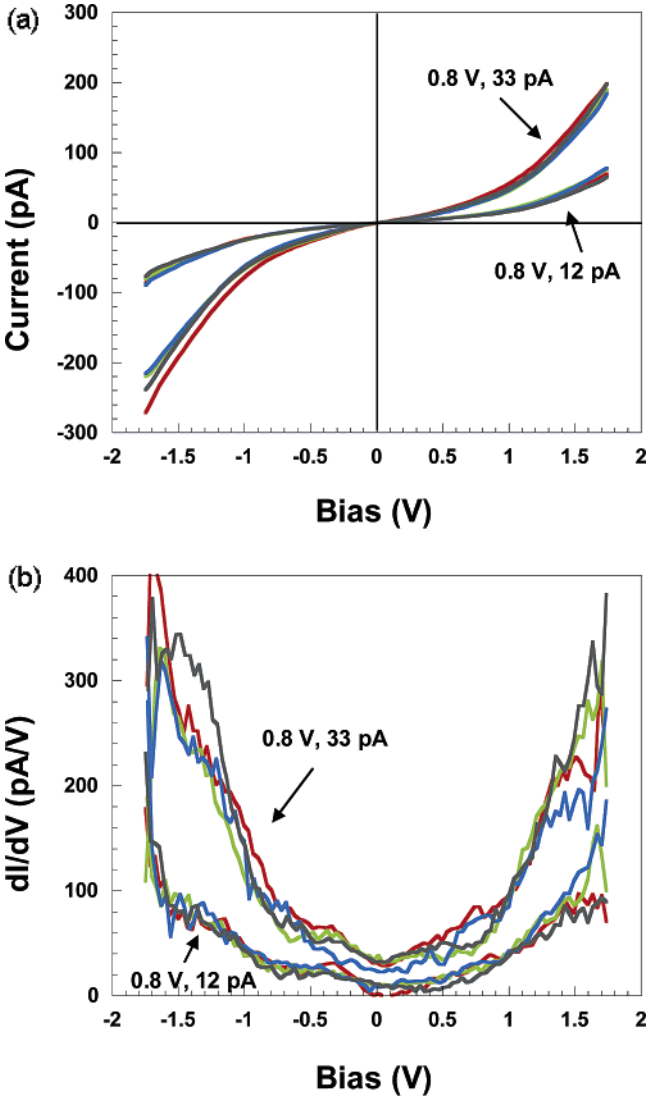

Figure 7. (a) $I-V$ and (b) the corresponding dI/d$V-V$ spectra recorded with the tip placed directly above designated termini. The spectra were acquired at the setpoints (0.8 V, 12 pA) and (0.8 V, 33 pA), as indicated in the figure, corresponding to tip$-CH_3$ separations of approximately 1.6 Å and 0.6 Å, respectively. A set of four curves are displayed for each setpoint, corresponding to the four nonequivalent molecules within the c(4×2) unit cell. The spectra corresponding to the same type of molecule are represented in the same color at both setpoints. The curves were only lightly smoothened, to preserve subtle spectroscopic features.

at a constant current. This trend can also be seen in Figure 3, which shows an $A_2 \rightarrow A_5$ contrast change upon either increasing I (Figure 3c,d) or decreasing V (Figure 3b,d). It will be shown in section C.3 that the transitions among all contrast types displayed in this diagram are completely reversible.

C.2. Correlation between STM Spectroscopy and the Contrast Diagram. To further understand the trend shown in Figure 6, we have acquired STM spectroscopy (STS) using two methods: (1) $I-V$ curves above the designated termini and (2) STM imaging at a series of I and V values corresponding to the same tip−SAM distance. Three relevant observations were made in this spectroscopic investigation. First, the $I-V$ spectra taken at the same setpoint appeared similar for the four nonequivalent molecules in the c(4×2) unit cell. Figure 7 shows $I-V$ and dI/d$V-V$ curves taken on top of the four nonequivalent molecules, at the setpoints (0.8 V, 12 pA) and (0.8 V, 33 pA), as indicated in the figure. The spectra corresponding to equivalent sites (i.e., same molecule type), are represented in the same color at both setpoints. The $I-V$ curves are slightly asymmetric, with higher currents at negative bias, the degree of asymmetry varying somewhat among molecules. The asymmetry likely arises from the nonequivalent coupling at the two junction ends (i.e., Au−S vs CH_3−vacuum-W tip); nonequivalent coupling may result in higher currents at either bias polarity, depending on the molecule species and the strength of the molecule-contact coupling.[67,68] This asymmetry was not observed for alkanedithiols, which are symmetric molecules, when coupled in symmetric junctions.[49,69] A more pronounced asymmetry in the $I-V$ spectra was reported for bulky and highly polarized termini such as $-CF_3$.[45]

The dI/d$V-V$ curves (Figure 7b) show peaks near ±0.5 V and near +1.5 V, which have been attributed previously to the Au(111) surface and to the alkanethiol SAM, respectively.[45] An additional peak is observed near −1.5 V, which was not reported previously for decanethiol SAMs.[45] The dI/d$V-V$ plot reveals some differences in LDOS among the four nonequivalent molecules in the c(4×2) unit cell. However, it is difficult to assign the observed contrast transitions to these dI/dV variations, as the signal-to-noise ratio in Figure 7b is not sufficient to reveal more details. A more reliable way is to extract the LDOS information from series of systematic STM images recorded with molecular resolution at the appropriate I and V conditions. Unlike $I-V$ curves, these images contain the distribution of LDOS over the whole SAM surface, from which we can compare the effects of LDOS under defined I and V conditions and at given sites within the unit cell.

The second observation was that the spectra recorded at various (I, V) setpoints were significantly different. Current−distance ($I-Z$) curves indicated that the setpoints (0.8 V, 12 pA) and (0.8 V, 33 pA) corresponded to tip$-CH_3$ distances of approximately 1.6 and 0.6 Å, respectively, following a previous report.[30] The difference in the slope of the two sets of $I-V$ curves shown in Figure 7a are thus rationalized by the difference in the gap resistance during the spectroscopy acquisition. The tip−termini separations for the $I-V$ spectra plotted in Figure 6, which were acquired at the setpoints (0.3 V, 10 pA) and (0.8 V, 16 pA) in the same experiment as the images in Figures 5 and 6, were approximately 0.5 and 1.3 Å, respectively.

Third, Figure 8b shows two series of STM images recorded at selected current and bias conditions along the two $I-V$ curves plotted in Figure 8a. The positive branches of these curves are also plotted in Figure 6. The $I-V$ spectra were recorded with the feedback off (i.e., holding the STM tip fixed above the SAM at the distance given by the setpoint); thus, all data points along the same $I-V$ curve represent combinations of bias and current corresponding to the same tip−sample separation. It is immediately evident that the same contrast type is encountered at the same tip-termini distance (i.e., only A_2 is observed at 1.3 Å and only A_3'' at 0.5 Å). This observation indicates that systematic, instead of random, trends are present in the contrast diagram shown in Figure 6. Indeed, plotting the $I-V$ curves and the various contrast types in Figure 6 clearly reveals that the STM spectra link the family of contrasts together. The rich contrast diagram displaying systematic contrast transitions and their correlation with the $I-V$ spectra are strong indications that the observed contrast variations originate from electronic effects (i.e., the LDOS of the SAM).

C.3. Reversibility in Contrast Transitions. Completely reversible and reproducible transitions have been observed in-situ for phase A among all contrasts shown in Figures 5 and 6. Six selected examples are shown in Figure 9. For a typical transition, the imaging conditions were first optimized for a

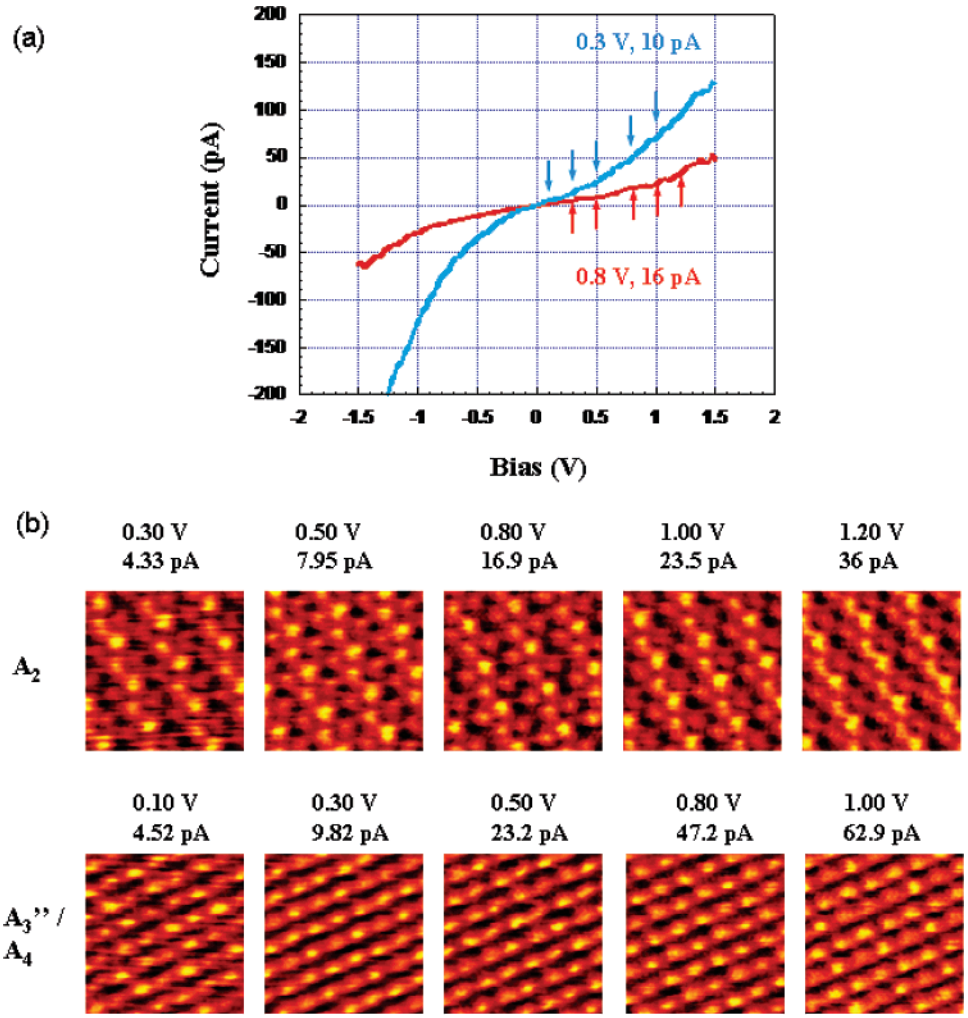

Figure 8. (a) Current−voltage ($I-V$) spectra taken at the setpoints (0.8 V, 16 pA) and (0.3 V, 10 pA), corresponding to tip-CH_3 separations of approximately 1.3 Å (red curve) and 0.5 Å (blue curve), respectively. (b) 30 × 30 Å STM images taken at combinations of bias and current which fall on the same $I-V$ curve. At a constant tip−CH_3 distance, the same STM contrast is encountered.

chosen contrast. Then, during the same frame and while scanning under the same bias, the current set point was quickly changed to another value resulting in an immediate contrast change in the next scanning line. The time for such change is less than 180 ms (line speed). The current set point was then changed back to the initial value, and the initial contrast was observed again within the same scan. The drift during scanning was insignificant in these experiments, as the initial and final lattices are in perfect alignment (Figure 9). Note that the same contrast transition can occur at different I and V settings (e.g., the $A_2 \leftrightarrow A_3'$ transitions in images in Figure 9b,c), which are also consistent with the trend shown in the contrast diagram (Figure 6). Reversible contrast changes were also observed upon changing the bias voltage, while keeping the current constant. Two examples are shown in Figure 10, where $A_5 \rightarrow A_3'' \rightarrow A_5$ (Figure 10a) and $A_4 \rightarrow A_3 \rightarrow A_4$ (Figure 10b) transitions occur upon variations in the bias voltage alone.

The contrast transitions shown in Figures 9 and 10 were observed during in situ imaging at molecular level with no drift during scanning. This enabled us to trace equivalent molecules systematically from one contrast type to another and to follow the evolution of their brightness, or apparent height, with imaging conditions. Thus, the unit cells shown in Figures 5, 9, and 10 are drawn in equivalent positions for all contrasts. An important observation can thus be made: depending on bias and current, three of the four molecules within the unit cell may exhibit the brightest STM contrast. For example, the corner thiols are brightest in A_1, the middle molecules appear brightest in A_2, and the corner becomes bright again in A_3. The largest change in apparent height occurs between contrasts A_3 and A_4 (Figures 5 and 10b): the corner molecule is 0.4 Å taller than the side one in contrast A_3 but is 0.3 Å shorter than the side molecule in A_4. These variations are within the range that can be caused by LDOS.[70]

It is very unlikely that such systematic and reversible contrast transitions (Figures 6 and 8−10) could be caused by completely reversible changes in (θ, χ, φ) under the influence of the STM tip, as suggested previously.[29,50,56] First, in Figures 9 and 10, reversible transitions are observed upon varying I or V within the same scan frame without any visible perturbations to the lattice. It would be very difficult to comprehend that zero-drift was observed during I or V changes in milliseconds if (θ, χ, φ) were altered. Second, the reversibility is observed upon both increasing and decreasing the tip−SAM interaction (decreasing and increasing impedance, respectively). Final evidence refuting the possibility of molecular reorientation will be presented in section C.4. Collectively, these results indicate that the STM contrast originates from the electronic structure of the molecules,

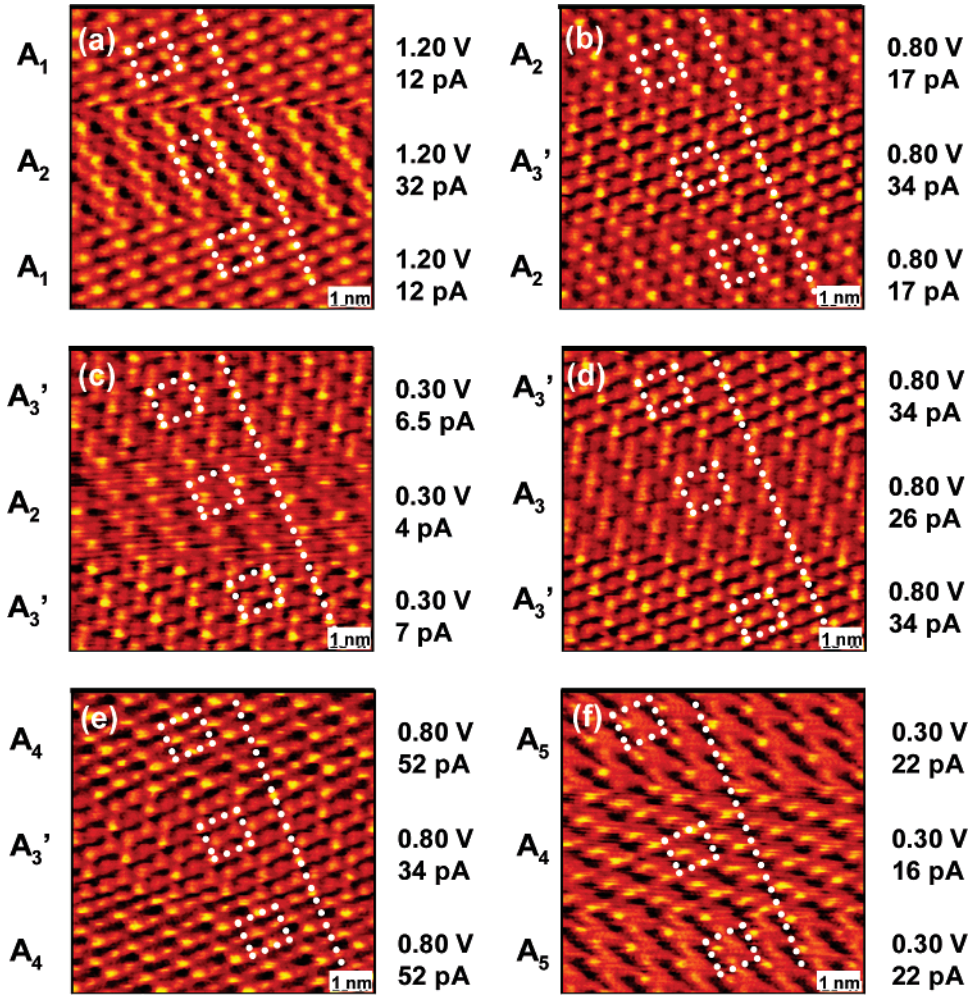

Figure 9. STM images showing reversible changes in contrast with varying the tunneling current at constant bias. The equivalent molecules can be traced systematically from one contrast type to another.

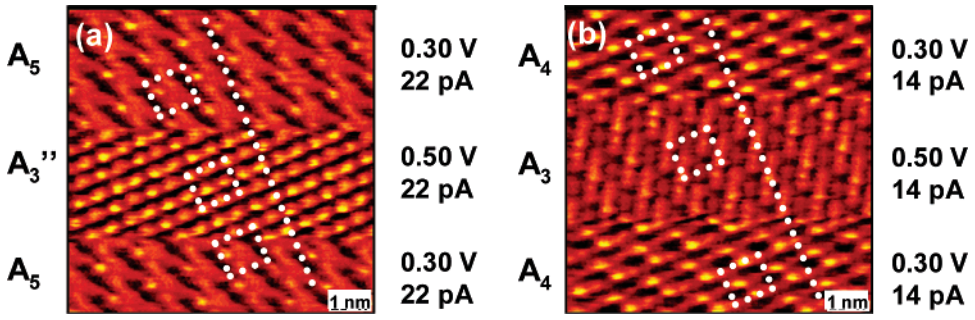

Figure 10. STM images showing reversible changes in contrast with varying the bias voltage at constant tunneling current. The equivalent molecules can be traced systematically from one contrast type to another.

and the contrast transitions are caused by probing the corresponding LDOS at given I and V. The LDOS difference among adsorbate molecules may originate from the hybridization state of the headgroup (sp vs sp^3),[46,65] from nonequivalent thiol adsorption sites (i.e., hollow, bridge, or top sites on Au(111))[46,65] and possibly from large variations in chain twist which may alter the chemisorption status.[54,65]

As shown in Figure 8b, the STM contrast does not show significant variations for bias voltages between +0.1 and +1.2 V at fixed tip−SAM separations. This is somewhat surprising at first glance, considering the rich LDOS structures expected for chemisorbed alkanethiols.[46,65] On the other hand, it is possible that the detailed electronic structure of the adsorbates cannot be detected when probed at several Å above the SAM, due to the fast decaying nature of the electron tunneling process. Using constant-height mode, Zeng et al.[46] also observed that the type of c(4×2) contrast did not change as the bias varied from −2.5 to +2.5 V at the same tip elevation, although the shape and intensity of the spots could vary significantly. Our observation of a well-defined contrast type at a fixed tip−surface distance (Figure 8b) is in agreement with those prior results. However, our systematic investigation of the contrast transitions (Figures 6 and 8−10), especially the observation the location of the brightest contrast within the unit cell depends on the imaging *I* and *V*, indicates that the LDOS contribution to the STM contrast is very important and can override the topographic differences in alkanethiol SAMs at specific imaging conditions. These new results contradict prior conclusions[46] that the SAM

topography dominates the STM contrast. It is likely that the range of tip−CH_3 distances surveyed in previous constant-height STM studies[46] was not sufficiently large to capture the variations due to LDOS. The importance of the tip−SAM distance to the STM contrast arising from LDOS was shown via DFT calculations[65] for individual alkanethiols chemisorbed on Au(111). To our knowledge, the results reported here represent the first experimental proof of this effect for alkanethiol SAMs.

C.4. Further Discussion on the LDOS versus Alternative Explanations for the Observed Contrast Transitions. Sections C.2 and C.3 presented our systematic investigations of the STM imaging contrast, which strongly support the explanation that LDOS is responsible for the observed contrast transitions. In this section, we discuss other alternative explanations for these transitions, such as stochastic switching and molecular reorientation.

Stochastic fluctuations in the STM contrast have been reported previously for alkanedithiols[71] or conjugated molecules[71,72] imbedded into alkanethiol SAMs. This random switching was attributed to molecular mobility,[71] changes in the molecular conformation, or tilt of the inserted molecules.[72] It was found that the switching frequency decreases with the increasing of long range order in the matrix alkanethiol SAMs.[72] Random switching within well-ordered regions of alkanethiols was not reported during the course of those experiments (several hours).[71,72] Stochastic fluctuations in the STM contrast of undecanethiol SAMs were not observed in our experiments either, as our SAMs were annealed and exhibit large domains of ordered thiols. It is likely that the frequency of random molecular reorientation is greatly reduced within the highly ordered and defect-free domains (Figure 3), where our images were recorded.[72]

Another alternative is explanation could be completely reversible and reproducible changes in (θ, χ, φ) during imaging. To check this possibility, we have analyzed the STM images and the tip-SAM interactions from the perspective of energy, to verify whether the contrast changes observed could be tip-induced transitions between c(4×2) structures of different energy minima.[54,55] Under constant bias and tunneling current, contrast changes were not observed during repeated imaging. Therefore, the thermal energy at room temperature ($kT = 0.6$ kcal/mol) is not sufficient to induce structural transformations. Other energy sources are the local electrical field and the thermal energy (or power, $I \times V$),during imaging. Considering all results presented thus far (Figures 5−10) and assuming that the tip-induced perturbation hypothesis is valid, three necessary conditions must be satisfied: (a) each molecular configuration is stable within a certain range of I and V (Figure 6) (i.e., under the corresponding strength of tip-SAM interactions); (b) the molecules can reorient reversibly between structures with different local energy minima (Figures 6, 9, and 10) upon changing the imaging conditions; (c) the change in field strength and/or power corresponding to a contrast transition should be larger than that within the same contrast family. The field strength, V/d, can be estimated for the images shown in Figure 8b, where d is the distance between the tip and the Au(111) surface. Taking a 30° chain tilt and 2.2 Å for the S−Au distance, the thickness of the undecanethiol SAM should be approximately 14.3 Å, not considering the height variations due to chain twist and S hybridization, which are insignificant in this estimation.[54] The resulting field strength corresponding to the two contrast series (Figure 8b) is within 0.98×10^9 to 0.77×10^9 V/m for A_2 and within 0.07×10^9 to 0.68×10^9 V/m for A_3'', the range overlapping for the two contrasts. As expected, all values are smaller than the 1.9×10^9 V/m required for field-induced desorption of alkanethiol SAMs. The thermal energy, or power estimated as $V \times I$, ranges between 1.3×10^{-12} and 43×10^{-12} W for A_2 and 0.45×10^{-12} and 62×10^{-12} W for A_3'', also overlapping for the two series of images. In other words, the contrast types follow the $I-V$ characteristics (Figures 6 and 8) and do not correspond to specific ranges of energy input by the STM tip. These observations are not consistent with the hypothesis that the contrast transitions could be due to tip-induced reversible changes in molecular orientation or (θ, χ, φ) variations.

Finally, electrostatic tip−termini interactions[45] could induce conformational changes at the SAM termini, even when changes in (θ, χ, φ) do not occur. Although the energy requirement in this case is small, this scenario is also unlikely to explain the numerous transitions between various c(4×2) contrasts. First, at the same tip-termini separation, the STM contrast does not change with varying the bias voltage in the range studied (Figure 8b). This is inconsistent with conformational changes induced by the polarization and tilting of the termini, which would vary with bias. Second, different contrasts are observed under the same energy input by the tip, which argues against the reversible reorientation of the termini as well, as discussed above for changes in (θ, χ, φ). Third, in the case of ($\sqrt{3}\times\sqrt{3}$)R30° structures present for as-deposited SAMs, the rich contrast transitions were not observed during imaging, although the tip-termini interactions are expected to be similar, if not identical, to the c(4×2) case. Finally, the electrostatic interactions between the negative tip (at positive bias on the sample) and positively charged CH_3 groups,[73] if important, would reduce the tip−termini distance. This would result in higher currents at positive bias, which are not observed in the $I-V$ spectra (Figure 7a). This evidence collectively indicates that the observed contrast transitions are not consistent with tip-induced termini reorientation.

D. STM Contrast Variations in Phase B. Phase B is another c(4×2) structure with four nonequivalent molecules per unit cell, whose STM contrast exhibits its own characteristics. Figure 11 shows a summary of the contrast types observed for phase B at different imaging conditions, displayed in order of increasing current and decreasing tip−CH_3 distance. Following the same discussion as for phase A, the c(4×2) unit cell in phase B is drawn for all contrasts with the corners on the same kind of the four nonequivalent molecules. Four main types of c(4×2) patterns were observed for this phase. Contrast B_1, observed at the highest impedances, is an ϵ-c(4×2) (Figure 1e). Contrast B_2 is the frequently observed δ-c(4×2) pattern (Figure 1d). Contrast B_2' is similar to B_2 but the molecule at the center of the long side of the unit cell has an increased apparent height, such that the aspect of this pattern is closer to the γ-c(4×2) (Figure 1c). Contrast B_3 is a β-c(4×2) pattern (Figure 1b), whereas B_4 is again a δ-c(4×2) pattern (Figure 1d), for which the bright zigzag rows are composed of a different pair of molecules than for B_2.

Figure 12 shows the contrast diagram for phase B, summarizing the dependence of the STM contrast on bias and current. Similarly to phase A, the contrast types observed for phase B are organized in separate domains. A systematic progression of contrast types with increasing current is observed again at each bias. For phase B, contrasts B_2 and B_2' take the same place in this progression, between B_1 and B_3, but they appear within different bias ranges. The dotted curves shown in this diagram are portions of current−voltage $I-V$ spectra recorded at the setpoints (0.8 V, 6 pA) and (0.8 V, 19 pA),

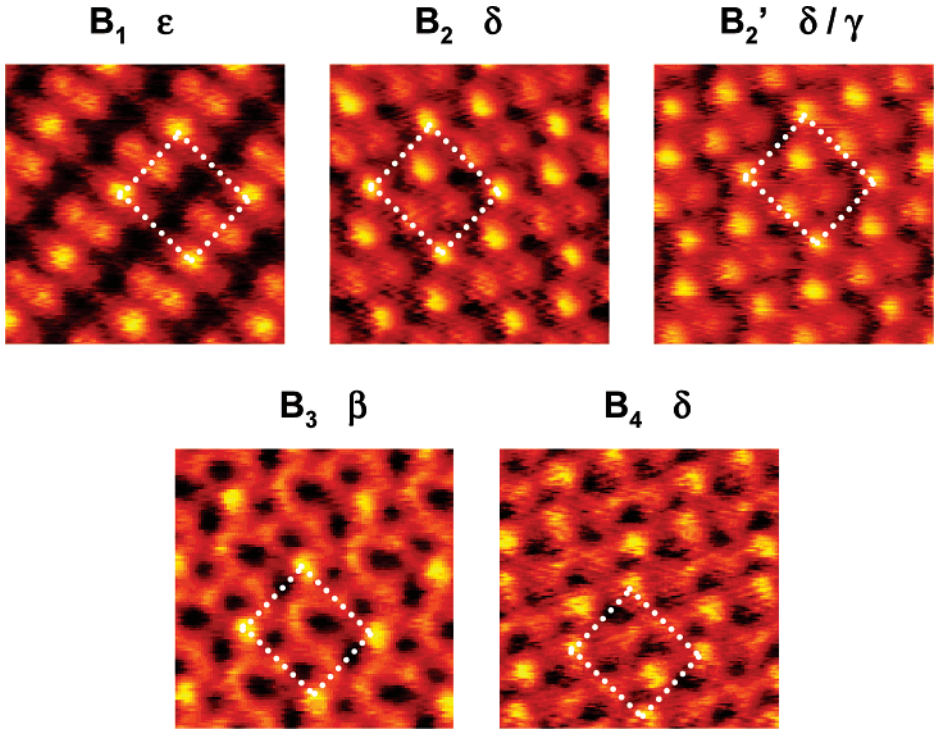

Figure 11. Summary of the contrast types observed by STM for phase B, 25 × 25 Å images. The c(4×2) unit cell is drawn with the corners on the same of the four nonequivalent molecule for all contrasts shown, as discussed in the text. Three nonequivalent molecules become the brightest in the unit cell, depending on the imaging conditions. B_1 (0.8 V, 5 pA), B_2 (0.8 V, 13 pA), B_2' (0.5 V, 9 pA), B_3 (0.8 V, 24 pA), B_4 (0.3 V, 25 pA).

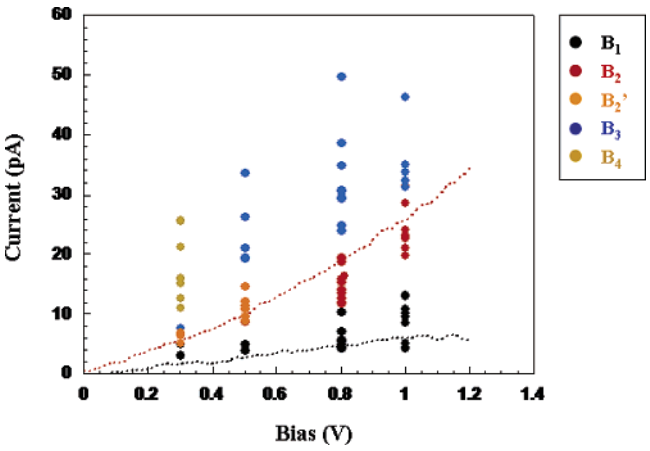

Figure 12. Contrast diagram for phase B as a function of bias and current. The dotted curves are portions of current−voltage ($I-V$) spectra taken at the setpoints (0.8 V, 6 pA) and (0.8 V, 19 pA), corresponding to tip-CH_3 separations of approximately 2.3 (black curve) and 1.1 Å (red curve), respectively.

corresponding to tip-CH_3 distances of approximately 2.3 and 1.1 Å, respectively.

Figure 13 shows two series of STM images recorded at bias and current combinations falling closely along the two $I-V$ curves shown in Figure 12. All images recorded at 2.3 Å display the same contrast, B_1, but both B_2 and B_2' are observed at 1.1 Å. These results support the conclusion that the variations in LDOS with the distance from the SAM are strong and can produce contrast transitions in STM. In addition, the observation of both B_2 and B_2' at 1.1 Å indicates that, for phase B, the LDOS also varies with bias voltage at this distance.

Figure 14 shows selected examples of contrast transitions observed for phase B. The molecule located on the corner of the unit cell (Figures 11 and 14) remains the brightest in all contrasts, whereas the two molecules inside the unit cell reverse brightness between contrasts B_2 and B_4, with a total change in relative apparent height of ~0.6 Å. This behavior supports the conclusion we already drew for phase A, that the STM contrast of alkanethiol SAMs and the contrast transitions originate from the LDOS of nonequivalent molecules. A small but consistent lateral shift is observed for the corner molecule in contrast B_1 with respect to B_2 and B_3 (Figure 14, panels a and d), which was not caused by drift but may be related to the orientation of the last C−C bond.[65]

Finally, the STM contrast of phase B does not have a marked dependence on either the field strength or the tip-induced power. For example, contrast B_1 is observed in Figure 13 for 0.18×10^9 to 0.60×10^9 V/m and 0.63×10^{-12} to 5.2×10^{-12} W, whereas B_2' is observed for 0.19×10^9 to 0.32×10^9 V/m and 1.95×10^{-12} to 4.45×10^{-12} W. As for phase A, this eliminates the possibility that the reversible contrast transitions observed for phase B may be due to tip-induced molecular reorientation.

Conclusions

A systematic UHV−STM investigation has been carried out to understand the rich STM contrast and the contrast transitions for alkanethiol SAMs. Annealed undecanethiol SAMs exhibit two structurally different c(4×2) phases coexisting on Au(111), as two STM contrasts were observed simultaneously under the same imaging conditions, which were referred to as *Phase A* and *Phase B*. This conclusion was further validated by comparing the manner in which the STM contrast varies with the imaging parameters for the two phases. The $(\sqrt{3}\times\sqrt{3})$R30° phase was not observed after annealing, indicating that the two c(4×2) structures are thermodynamically more stable than the basic $(\sqrt{3}\times\sqrt{3})$R30°, in agreement with previous studies.

We observed systematic, reversible, and reproducible contrast transitions with bias and current. It was concluded that these contrast transitions are caused by probing the corresponding

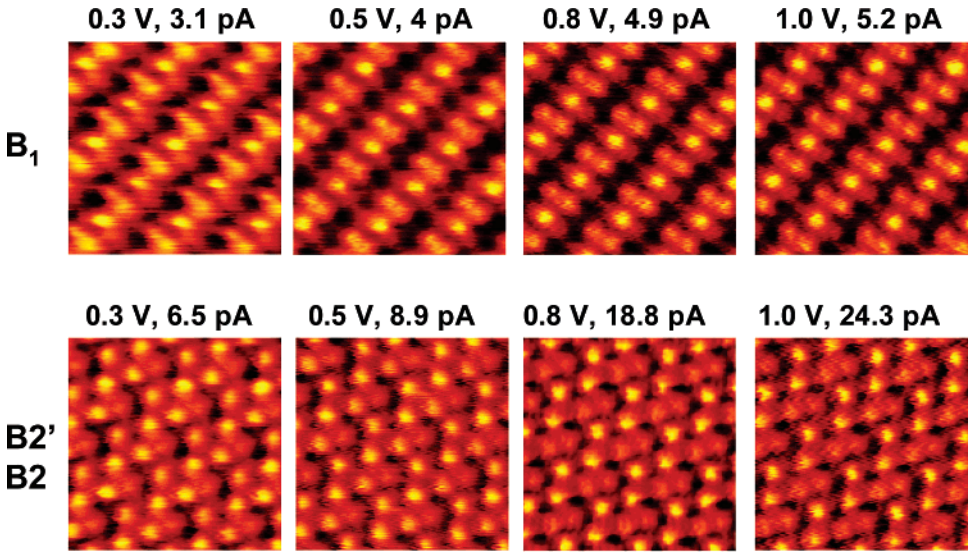

Figure 13. 30 × 30 Å STM scans taken at combinations of bias and current which follow the same $I(V)$ curve. At a constant tip−CH_3 distance, the same contrast is encountered.

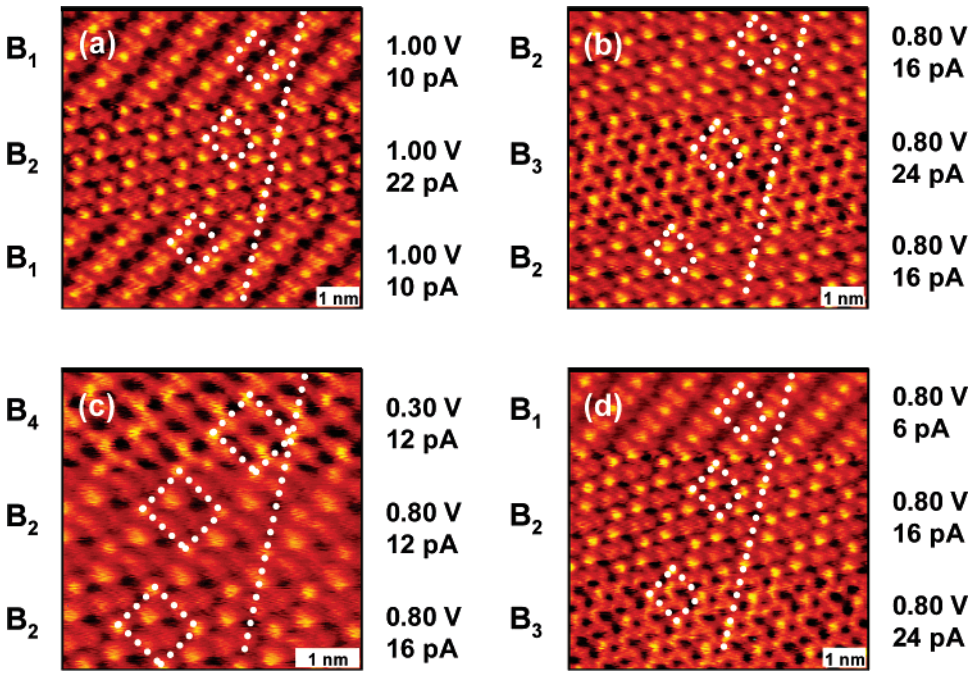

Figure 14. STM images showing reversible changes in contrast with varying the tunneling current at constant bias. The equivalent molecules can be traced systematically from one contrast type to another.

LDOS upon variation of the tunneling conditions, and not by the reorientation of the molecules during scanning. The two c(4×2) phases manifest into rich contrast diagrams as various LDOS are captured by STM at defined I, V, and tip−CH_3 separations. Various contrast families correlate well the corresponding $I-V$ spectra. It was found that the STM contrast is very sensitive to the tip−CH_3 separation due to changes in LDOS with the distance above the SAM. This effect had been predicted by theory for this system but not observed or investigated systematically prior to this work. The contribution to the STM contrast brought by variations in LDOS can surpass the difference in physical height between molecules. At given tip−CH_3 separations, the LDOS probed by STM between +0.1 and +1.2 V bias voltage does not vary much for undecanethiols. These systematic investigations demonstrate the significant role played by LDOS in the STM contrast of alkanethiols.

Acknowledgment. We thank Dr. Giulia Galli, Dr. Yan Li, Mr. Christopher Fleming, and Ms. Susan G. Stagner at University of California, Davis for helpful discussions. This work was supported by the University of California, Davis, and National Science Foundation under the Grant CHE 0244830 and a seed fund from CPIMA via Stanford University (NSF-MRSEC DMR-0213618).

References and Notes

(1) Schreiber, F. *Prog. Surf. Sci.* **2000**, *65*, 151.
(2) Tour, J. M. *Acc. Chem. Res.* **2000**, *33*, 791.
(3) Joachim, C.; Gimzewski, J. K.; Aviram, A. *Nature (London)* **2000**, *408*, 541.
(4) Pease, A. R.; Jeppesen, J. O.; Stoddart, J. F.; Luo, Y.; Collier, C. P.; Heath, J. R. *Acc. Chem. Res.* **2001**, *34*, 433.
(5) McCreery, R. L. *Chem. Mater.* **2004**, *16*, 4477.
(6) Komvopoulos, K. *Wear* **1996**, *200*, 305.

(7) Maboudian, R.; Ashurst, W. R.; Carraro, C. *Tribol. Lett.* **2002**, *12*, 95.
(8) Alivisatos, A. P.; Barbara, P. F.; Castleman, A. W.; Chang, J.; Dixon, D. A.; Klein, M. L.; McLendon, G. L.; Miller, J. S.; Ratner, M. A.; Rossky, P. J.; Stupp, S. I.; Thompson, M. E. *Adv. Mater.* **1998**, *10*, 1297.
(9) Crooks, R. M.; Ricco, A. J. *Acc. Chem. Res.* **1998**, *31*, 219.
(10) Flink, S.; van Veggel, F.; Reinhoudt, D. N. *Adv. Mater.* **2000**, *12*, 1315.
(11) Willner, I.; Katz, E. *Angew. Chem.-Int. Ed.* **2000**, *39*, 1180.
(12) Mrksich, M.; Chen, C. S.; Xia, Y. N.; Dike, L. E.; Ingber, D. E.; Whitesides, G. M. *Proc. Natl. Acad. Sci. U.S.A.* **1996**, *93*, 10775.
(13) Deng, L.; Mrksich, M.; Whitesides, G. M. *J. Am. Chem. Soc.* **1996**, *118*, 5136.
(14) Wadu-Mesthrige, K.; Amro, N. A.; Liu, G. Y. *Scanning* **2000**, *22*, 380.
(15) Wadu-Mesthrige, K.; Amro, N. A.; Garno, J. C.; Xu, S.; Liu, G. Y. *Biophys. J.* **2001**, *80*, 1891.
(16) Liu, G. Y.; Amro, N. A. *Proc. Natl. Acad. Sci. U.S.A.* **2002**, *99*, 5165.
(17) Camillone, N.; Chidsey, C. E. D.; Eisenberger, P.; Fenter, P.; Li, J.; Liang, K. S.; Liu, G. Y.; Scoles, G. *J. Chem. Phys.* **1993**, *99*, 744.
(18) Fenter, P.; Eisenberger, P.; Liang, K. S. *Phys. Rev. Lett.* **1993**, *70*, 2447.
(19) Torrelles, X.; Barrena, E.; Munuera, C.; Rius, J.; Ferrer, S.; Ocal, C. *Langmuir* **2004**, *20*, 9396.
(20) Fenter, P.; Eberhardt, A.; Liang, K. S.; Eisenberger, P. *J. Chem. Phys.* **1997**, *106*, 1600.
(21) Strong, L.; Whitesides, G. M. *Langmuir* **1988**, *4*, 546.
(22) Camillone, N.; Chidsey, C. E. D.; Liu, G. Y.; Scoles, G. *J. Chem. Phys.* **1993**, *98*, 3503.
(23) Chidsey, C. E. D.; Liu, G. Y.; Rowntree, P.; Scoles, G. *J. Chem. Phys.* **1989**, *91*, 4421.
(24) Nuzzo, R. G.; Korenic, E. M.; Dubois, L. H. *J. Chem. Phys.* **1990**, *93*, 767.
(25) Nuzzo, R. G.; Dubois, L. H.; Allara, D. L. *J. Am. Chem. Soc.* **1990**, *112*, 558.
(26) Barrena, E.; Ocal, C.; Salmeron, M. *J. Chem. Phys.* **2001**, *114*, 4210.
(27) Fukuma, T.; Ichii, T.; Kobayashi, K.; Yamada, H.; Matsushige, K. *J. Appl. Phys.* **2004**, *95*, 1222.
(28) O'Dwyer, C.; Gay, G.; de Lesegno, B. V.; Weiner, J. *Langmuir* **2004**, *20*, 8172.
(29) Touzov, I.; Gorman, C. B. *J. Phys. Chem. B* **1997**, *101*, 5263.
(30) Yang, G. H.; Liu, G. Y. *J. Phys. Chem. B* **2003**, *107*, 8746.
(31) Qian, Y. L.; Yang, G. H.; Yu, J. J.; Jung, T. A.; Liu, G. Y. *Langmuir* **2003**, *19*, 6056.
(32) Poirier, G. E.; Tarlov, M. J. *Langmuir* **1994**, *10*, 2853.
(33) Poirier, G. E.; Pylant, E. D. *Science* **1996**, *272*, 1145.
(34) Poirier, G. E. *Langmuir* **1999**, *15*, 1167.
(35) Poirier, G. E.; Fitts, W. P.; White, J. M. *Langmuir* **2001**, *17*, 1176.
(36) Delamarche, E.; Michel, B.; Kang, H.; Gerber, C. *Langmuir* **1994**, *10*, 4103.
(37) Delamarche, E.; Michel, B.; Gerber, C.; Anselmetti, D.; Guntherodt, H. J.; Wolf, H.; Ringsdorf, H. *Langmuir* **1994**, *10*, 2869.
(38) Delamarche, E.; Michel, B.; Biebuyck, H. A.; Gerber, C. *Adv. Mater.* **1996**, *8*, 719.
(39) Bucher, J. P.; Santesson, L.; Kern, K. *Appl. Phys. A-Mater. Sci. Process.* **1994**, *59*, 135.
(40) Schonenberger, C.; Jorritsma, J.; Sondaghuethorst, J. A. M.; Fokkink, L. G. J. *J. Phys. Chem.* **1995**, *99*, 3259.
(41) Noh, J.; Nakajima, K.; Hara, M.; Sasabe, H.; Knoll, W.; Lee, H. *Korea Polym. J.* **1998**, *6*, 307.
(42) Noh, J.; Hara, M. *Langmuir* **2001**, *17*, 7280.
(43) Noh, J.; Hara, M. *Langmuir* **2002**, *18*, 1953.
(44) Noh, J.; Kato, H. S.; Kawai, M.; Hara, M. *J. Phys. Chem. B* **2006**, *110*, 2793.
(45) Pflaum, J.; Bracco, G.; Schreiber, F.; Colorado, R.; Shmakova, O. E.; Lee, T. R.; Scoles, G.; Kahn, A. *Surf. Sci.* **2002**, *498*, 89.
(46) Zeng, C. G.; Li, B.; Wang, B.; Wang, H. Q.; Wang, K. D.; Yang, J. L.; Hou, J. G.; Zhu, Q. S. *J. Chem. Phys.* **2002**, *117*, 851.
(47) Kakiuchi, T.; Iida, M.; Gon, N.; Hobara, D.; Imabayashi, S.; Niki, K. *Langmuir* **2001**, *17*, 1599.
(48) Kawasaki, M.; Sato, T.; Tanaka, T.; Takao, K. *Langmuir* **2000**, *16*, 1719.
(49) Kobayashi, K.; Yamada, H.; Horiuchi, T.; Matsushige, K. *Jpn. J. Appl. Phys. Part 1* **1998**, *37*, 6183.
(50) Vericat, C.; Andreasen, G.; Vela, M. E.; Martin, H.; Salvarezza, R. C. *J. Chem. Phys.* **2001**, *115*, 6672.
(51) Vericat, C.; Vela, M. E.; Salvarezza, R. C. *Phys. Chem. Chem. Phys.* **2005**, *7*, 3258.
(52) Lussem, B.; Muller-Meskamp, L.; Karthauser, S.; Waser, R. *Langmuir* **2005**, *21*, 5256.
(53) Mar, W.; Klein, M. L. *Langmuir* **1994**, *10*, 188.
(54) Li, T. W.; Chao, I.; Tao, Y. T. *J. Phys. Chem. B* **1998**, *102*, 2935.
(55) Pertsin, A. J.; Grunze, M. *Langmuir* **1994**, *10*, 3668.
(56) Arce, F. T.; Vela, M. E.; Salvarezza, R. C.; Arvia, A. J. *J. Chem. Phys.* **1998**, *109*, 5703.
(57) Beardmore, K. M.; Kress, J. D.; Gronbech-Jensen, N.; Bishop, A. R. *Chem. Phys. Lett.* **1998**, *286*, 40.
(58) Gottschalck, J.; Hammer, B. *J. Chem. Phys.* **2002**, *116*, 784.
(59) Gronbeck, H.; Curioni, A.; Andreoni, W. *J. Am. Chem. Soc.* **2000**, *122*, 3839.
(60) Morikawa, Y.; Hayashi, T.; Liew, C. C.; Nozoye, H. *Surf. Sci.* **2002**, *507*, 46.
(61) Vargas, M. C.; Giannozzi, P.; Selloni, A.; Scoles, G. *J. Phys. Chem. B* **2001**, *105*, 9509.
(62) Yourdshahyan, Y.; Zhang, H. K.; Rappe, A. M. *Phys. Rev. B* **2001**, *6308*.
(63) Yourdshahyan, Y.; Rappe, A. M. *J. Chem. Phys.* **2002**, *117*, 825.
(64) Fenter, P.; Eberhardt, A.; Eisenberger, P. *Science* **1994**, *266*, 1216.
(65) Li, B.; Zeng, C. G.; Li, Q. X.; Wang, B.; Yuan, L. F.; Wang, H. Q.; Yang, J. L.; Hou, J. G.; Zhu, Q. S. *J. Phys. Chem. B* **2003**, *107*, 972.
(66) Selloni, A.; Carnevali, P.; Tosatti, E.; Chen, C. D. *Phys. Rev. B* **1985**, *31*, 2602.
(67) Kushmerick, J. G.; Holt, D. B.; Yang, J. C.; Naciri, J.; Moore, M. H.; Shashidhar, R. *Phys. Rev. Lett.* **2002**, *89*.
(68) Zahid, F.; Ghosh, A. W.; Paulsson, M.; Polizzi, E.; Datta, S. *Phys. Rev. B* **2004**, *70*.
(69) Li, X. L.; He, J.; Hihath, J.; Xu, B. Q.; Lindsay, S. M.; Tao, N. J. *J. Am. Chem. Soc.* **2006**, *128*, 2135.
(70) Lu, X.; Hipps, K. W.; Wang, X. D.; Mazur, U. *J. Am. Chem. Soc.* **1996**, *118*, 7197.
(71) Ramachandran, G. K.; Hopson, T. J.; Rawlett, A. M.; Nagahara, L. A.; Primak, A.; Lindsay, S. M. *Science* **2003**, *300*, 1413.
(72) Donhauser, Z. J.; Mantooth, B. A.; Kelly, K. F.; Bumm, L. A.; Monnell, J. D.; Stapleton, J. J.; Price, D. W.; Rawlett, A. M.; Allara, D. L.; Tour, J. M.; Weiss, P. S. *Science* **2001**, *292*, 2303.
(73) Evans, S. D.; Ulman, A. *Chem. Phys. Lett.* **1990**, *170*, 462.